

Article

Improved Plasticity of Ti-Based Bulk Metallic Glass at Room Temperature by Electroless Thin Nickel Coating

Xin Wang * , Ximei Hu, Lichen Zhao, Dongxu Jiang, Peng Chen, Pengdong Wang, Zhipeng Zhang, Shuiqing Liu and Chunxiang Cui *

Key Laboratory for New Type of Functional Materials in Hebei Province, School of Material Science and Engineering, Hebei University of Technology, Tianjin 300130, China; huximei@hebut.edu.cn (X.H.); zhlch@hebut.edu.cn (L.Z.); 15022635520@163.com (D.J.); m15900225021@163.com (P.C.); 18322518030@163.com (P.W.); zhang_zhipeng123@163.com (Z.Z.); liushuiqing0824@126.com (S.L.)

* Correspondence: ahaxin@hebut.edu.cn (X.W.); hutcui@hebut.edu.cn (C.C.);

Tel.: +86-022-6020-2194 (X.W.); +86-022-2656-4125 (C.C.); Fax: +86-022-6020-4125 (X.W. & C.C.)

Received: 4 November 2017; Accepted: 6 December 2017; Published: 14 December 2017

Abstract: By restricting the dilated deformation, surface modification can stimulate multiple shear banding and improve the plasticity of bulk metallic glasses (BMGs). Aimed at modifying the surface of BMGs by thin layers, a crystalline Ni coating with ultrafine grains was coated on the surface of a Ti-based BMG by electroless plating. With a thickness of about 10 μm , the prepared thin coating could effectively limit the fast propagation of primary shear bands and stimulate the nucleation of multiple shear bands. As a result, the compression plasticity of the coated Ti-based BMG was improved to about 3.7% from near 0% of the non-coated BMG. Except for a small amount of Ni coating was adhered to the BMG substrate after fracture, most of the coatings were peeled off from the surface. It can be attributed to the abnormal growth of some coarse grains/particles in local region of the coating, which induces a large tensile stress at the interface between the coating and the BMG substrate. It is suggested that, for electroless nickel plating, improving the adhesive bonding strength between the coating and the substrate has a better geometric restriction effect than simply increasing the thickness of the coating.

Keywords: bulk metallic glass; titanium alloy; electroless plating; Ni coating; plasticity

1. Introduction

Titanium-based bulk metallic glasses (BMGs) are rapidly developing glassy alloy systems in recent years due to the requirement of lightweight metals in modern industries [1–3]. The specific strength values of Ti-based BMGs are universally over $3.5 \times 10^5 \text{ N m kg}^{-1}$, which is significantly higher than the typical titanium alloy Ti-6Al-4V ($2.6 \times 10^5 \text{ N m kg}^{-1}$) [4,5]. Ti-based BMGs also have many other outstanding properties, including good corrosion resistance [6,7], good biocompatibility [8–10], and good glass-forming-ability (GFA) [11,12], having potential applications in the fields of consumer electronics, automotive, biomedical devices, aerospace, and so on [13,14]. However, some Ti-based BMGs, especially the alloys with compositions within the range of best GFA in each alloy system, often show brittle deformation behaviors and the compression plasticity at room temperature is poor. For example, among Ti-Zr-Be-Fe-Cu BMG alloys, the GFA of $\text{Ti}_{37.31}\text{Zr}_{22.75}\text{Be}_{25.48}\text{Fe}_{5.46}\text{Cu}_9$ BMG is the best one, and the critical size of as-cast rod with full glassy structure is $>32 \text{ mm}$ in diameter, but its plasticity is relatively poor (less than 1%) [12]. If the Cu or Fe content of Ti-Zr-Be-Fe-Cu alloys changes (so-called alloying), then the plasticity would be greatly improved but the GFA would be obviously decreased [12,15,16]. For high strength structural materials, certain plasticity usually is required not

only for mechanical property, but also for service safety [17]. Therefore, how to improve the plasticity is a challenge in Ti-based BMGs for further applications.

Surface modification is an effective method to extrinsically improve the plasticity of BMGs [18]. On the one hand, surface modification technologies, including shot peening [19], surface mechanical attrition treatment (SMAT) [20], magnetron sputtering [21], laser processing [22], and conventional electroplating [23], or electroless plating [24], and so on, would make residual compression stresses on the surface of BMGs, affecting the shear banding processes, including the shear band nucleation and the shear band propagation [25,26]. In 2007, Li et al. firstly deposited a Ni-15% Fe coating on the surface of a Zr-based BMG by electroplating, and the compression plasticity of the deposited BMG was improved from about 1.1% to ~2.0% [23]. Yu et al. used Cu tubes as geometric constraints to improve the plasticity of a Zr-based BMG, hereafter, the surface modification strategy was often called geometric constraint method [27]. Following similar strategy, Qiu et al. used electroplating to coat Zr-based BMG with Cu coating, and found that the thicker coating shows greater toughening effect [28]. Then, the thickening of the coating become the focus in such studies, stimulating the development of Cu/Ni composite coating [29]. As the Cu coating reached 160 μm or more, the coating did not even break after the failure of the coated BMG sample [30]. However, the weight of the coated sample would be increased with thick coatings, which must be disadvantageous to the lightweight development of BMGs. Therefore, the thin coating or lightweight coating should be taken for granted. It is known that electroless Ni coating generally is thinner than the electroplating Ni coating, meanwhile, the mechanical properties of the coating can be controlled by turning the chemical composition or the grain size [31,32]. For sufficient geometric constrain, the thickness of electroless Ni coating may not need a large value. For example, the plasticity of Fe-based BMGs can be significantly improved by a very thin electroless Ni coating (~6 μm) [24]. So far, electroless Ni plating has been used in Zr-based [33], Fe-based BMGs [24], and high entropy alloy [34], not yet in Ti-based BMGs.

In the present work, a $\text{Ti}_{37.31}\text{Zr}_{22.75}\text{Be}_{25.48}\text{Fe}_{5.46}\text{Cu}_9$ BMG [12] was coated with thin Ni coating by electroless plating. The microstructure of the Ni coating and the effect of the coating on improving the plasticity of Ti-based BMG were investigated.

2. Materials and Methods

2.1. Preparation of BMG Rods

For preparing the BMG with nominal composition of $\text{Ti}_{37.31}\text{Zr}_{22.75}\text{Be}_{25.48}\text{Fe}_{5.46}\text{Cu}_9$ [12], high purity materials, including Ti (99.4 wt. %), Zr (99.7 wt. %), Be (99.9 wt. %), Cu (99.99 wt. %), and Fe (99.9 wt. %) were melted together by arc melting under high purity Ar protection. In order to ensure the homogeneity of the master alloy, the ingots were upside down and re-melted for at least four times. Then, the ingots were re-melted by induction melting in a quartz tube and injected into a copper mold with a cavity of 2 mm in diameter and 100 mm in height. This technology is so-called injection casting and the schematic diagram of the used equipment was shown elsewhere [35]. The as-cast rod was broken to two parts from the middle region, one part was used for electroless plating and the other one was used for comparison. The amorphous structure of the as-cast sample were confirmed by an X-ray diffractometer (XRD, Bruker D8 Advance; Bruker, Karlsruhe, Baden-Württemberg, Germany) at a scanning rate of 8°/min, using Cu K α target.

2.2. Preparation of Electroless Ni Coating

For electroless plating, the detailed technology follows the route displayed in Figure 1. Firstly, the as-cast rod was ground with fine sandpaper #2000 using a small slow lathe, for removing the casting defects and oxide layers. Then, the rod was cleaned with acetone under ultrasonic treatment for 15 min. Secondly, for the coarsing treatment by acid pickling, the cleaned sample was immersed in a 5% HF aqueous solution and was kept for 2 min to roughen the surface. Thirdly, the roughened samples were sensitized in a solution with a composition of HCl 40 mL/L and SnCl_2 30 g/L for about

20 min (unless otherwise specified, chemical reagents that are used in this work are analytical reagents). Fourthly, the re-cleaned samples were immersed in an activation solution (PdCl_2 0.5 g/L, HCl 60 mL/L) for 20 min to pre-plate a very thin Pd layer on the surface of the BMG rod. Finally, after cleaning by a reducing agent ($\text{NaH}_2\text{PO}_2 \cdot \text{H}_2\text{O}$ 20 g/L) and deionized water in turn, the activated BMG rod was hanged in the bath without contacting the wall of the container, plating for about 1 h at a temperature of about 80 °C. The bath is a mixture solution of $\text{NiSO}_4 \cdot 6\text{H}_2\text{O}$ 30 g/L, $\text{NaH}_2\text{PO}_2 \cdot \text{H}_2\text{O}$ 20 g/L, $\text{NaC}_6\text{H}_5\text{O}_7 \cdot 2\text{H}_2\text{O}$ 30 g/L, CH_3COONa 15 g/L, NaF 1.5 g/L, $\text{C}_{12}\text{H}_{25}\text{SO}_4\text{Na}$ 0.1 g/L, and Na_2MoO_4 0.1 g/L. The pH value of the bath was adjusted to 9.0 by a pH meter (PHS-3CB; Shanghai Yueping Scientific Instrument Co., Ltd., Shanghai, China), using saturated sodium hydroxide solution. The surface morphology, interface microstructure and chemical composition of the coating were examined by a scanning electron microscope (SEM, Hitachi S-4800; Hitachi, Tokyo, Japan) and an energy dispersive spectrometer (EDS; EDAX, Mahwah, NJ, USA). The phase structure of the coating was investigated by an XRD (Bruker D8 Advance; Bruker, Karlsruhe, Baden-Württemberg, Germany) at a scanning rate of 8°/min.

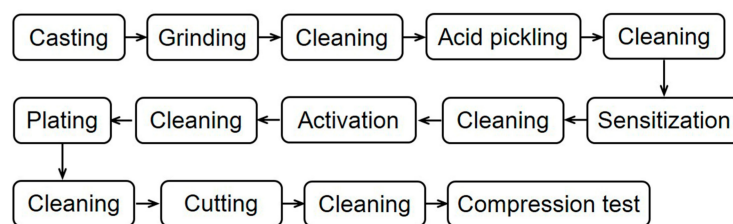


Figure 1. The process diagram of the electroless Ni plating.

2.3. Compression Test

The Ni-coated rod was cut into compression samples by a slow diamond cutting machine (SYJ120; Shenyang Kejing Auto-instrument Co., Ltd., Shenyang, China). The speed of the cutter was set to 90 rpm, using special coolant for lubrication and cooling to avoid excessive damage of the coating. For each compression sample, the length was cut as longer than 4 mm, ensuring that the ratio of height and diameter is over about 2:1, in agreement with ASTM E9-89a. The quasi-static compression tests were performed on an electronic universal testing machine (WDW-10KN; Jilin Guanteng Automation Technology Co., Ltd., Changchun, China), with a deformation rate of 0.05 mm/min. The fracture surface and the side surface of the deformed samples were analyzed by SEM (Hitachi S-4800; Hitachi, Tokyo, Japan).

3. Results

3.1. Preparation of Electroless Ni Coating

Figure 2a shows the layered structure of the electroless coating on the surface of the as-cast $\text{Ti}_{37.31}\text{Zr}_{22.75}\text{Be}_{25.48}\text{Fe}_{5.46}\text{Cu}_9$ BMG rod. The picture is taken from a region near the cross-section surface produced by the cutting. The fracture surface of the coating is artificially made by using a horseshoe knife. It is found that the coating has two layers, in which the outer layer is thicker. Figure 2b shows the surface morphology of the outer coating, it can be clearly seen that there are many particle-like materials on the surface of the BMG rod, covering the scratches that are induced by the grinding treatment. The size of the bigger particles in the coating shown in Figure 2b is about $\sim 2 \mu\text{m}$, and the size of the smaller particles is about 500 nm, as shown in Figure 2c. In addition, the thickness of the inner coating is relatively smaller than the outer coating and the coating is adhesive to the surface of BMG rod, even after removing the outer coating. It is suggested that the bonding between the inner layer and the BMG substrate might be strong. Figure 2d also shows the surface morphology of the inner coating, revealing that the size of the particles in the inner coating is about 100 nm, very smaller than that of outer coating. Therefore, it is demonstrated that the coated alloy has very fine grains.

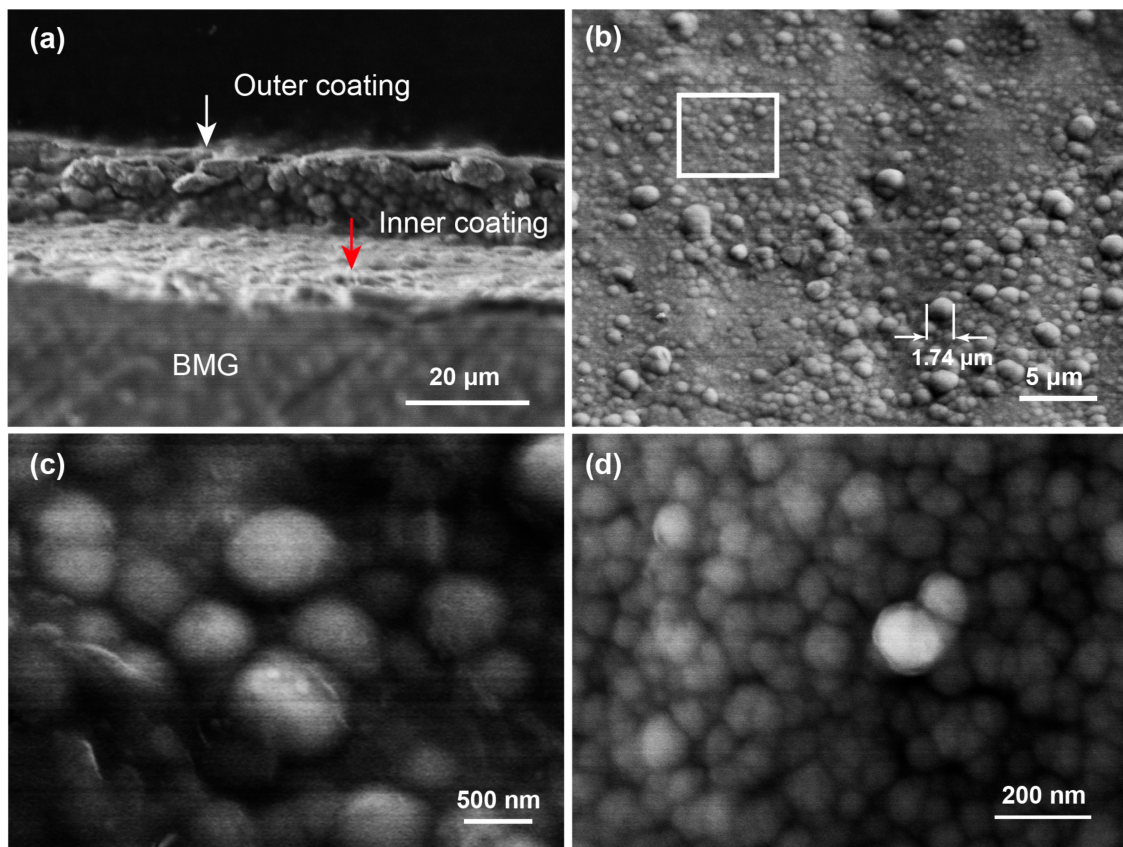


Figure 2. Scanning electron microscope (SEM) images showing the morphology of the electroless Ni coating on the surface of Ti-based BMG rod. (a) SEM image of the peeling off part showing layered structure of the coating; (b) Surface morphology of the outer coating; (c) Higher magnification image on the white square in (b); and, (d) Surface morphology of the outer coating.

Figure 3a shows a typical cross-sectional image of the electroless plated BMG sample, from which the thickness of the coating can be measured as $\sim 10 \mu\text{m}$. This cross-sectional surface is actually the kerf produced by the diamond saw, showing that the cutting process did not make the coating peel off from the BMG rod. Moreover, there is no obvious gap between the coating and the BMG substrate. Therefore, in our opinion, it is implied that the adhesive bonding strength between the coating and the BMG substrate might be good. In order to analyze the element distribution on the coating, a line EDS scanning is performed along the white line that is marked in Figure 3a, and the result is shown in Figure 3b. Within the range of the coating, the intensity of the EDS spectrum of Ni is significantly higher than that in the other ranges, indicating that the coating is rich in Ni. The high Ni-content range is about $10 \mu\text{m}$, in agreement with the thickness of the Ni coating, as shown in Figures 2a and 3a. Since line EDS scanning cannot provide the detailed composition information, point EDS testing performed on the coating (Red cross marked by C) and the BMG matrix (Red cross marked by D) is carried out and the results are shown in Figure 3c,d, respectively. It is obvious that the matrix contains no P and almost no Ni, and the coating contains certain amounts of Ni and P. Therefore, the prepared electroless coating actually is a Ni-P coating. In addition, the intensity of the O spectrum in the coating and the substrate range almost has no change, showing that the coating contains a low amount of O.

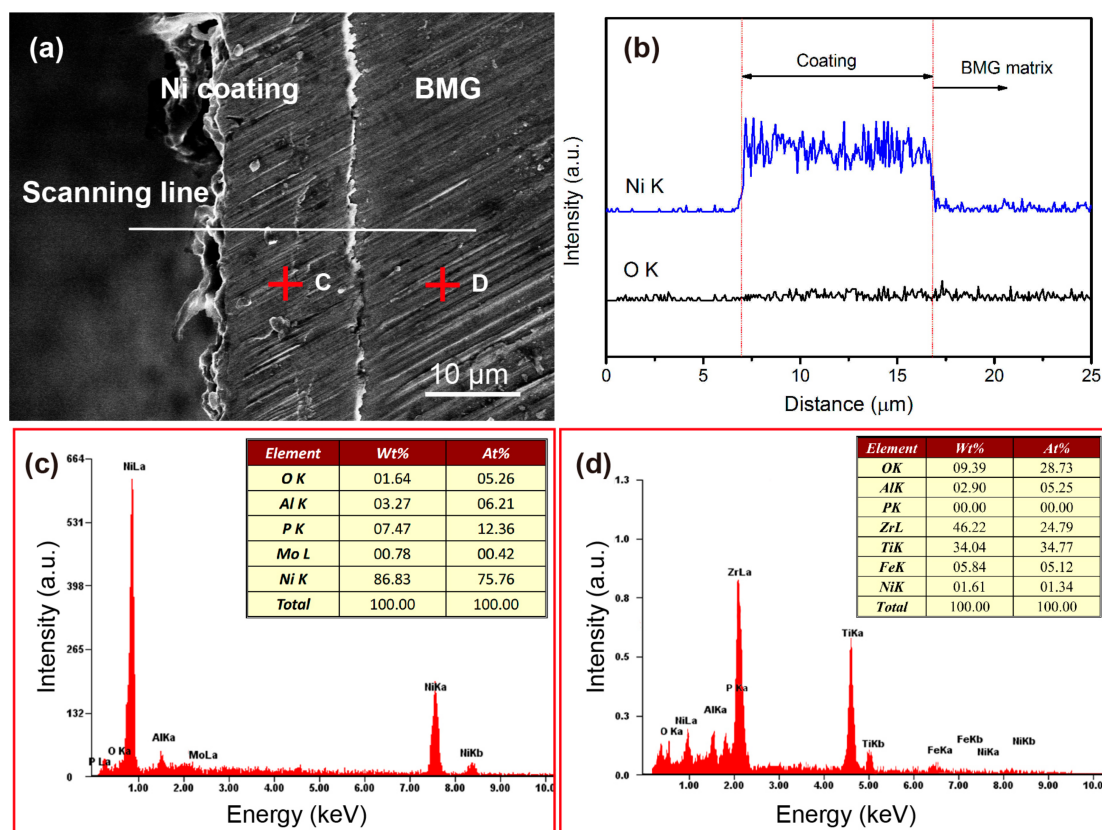


Figure 3. (a) Typical SEM image of the cross-section of the coated bulk metallic glasses (BMG) rod; (b) energy dispersive spectrometer (EDS) line scanning results performed along the white line marked in (a); (c) EDS spectrum of the point testing performed on cross C in (a); and, (d) EDS spectrum of the point testing performed on cross D in (a) together with the corresponding elemental analysis results.

Figure 4 shows the XRD spectrum that is performed on the surface of the coated BMG sample, when compared with the non-coated BMG sample. Before electroless Ni-plating, the XRD spectrum of the BMG rod has the typical features of amorphous materials, that is, there is no sharp diffraction peaks corresponding to any crystalline phase and only a diffuse peak at 2θ of $35\text{--}42^\circ$, similar to the previous work [12]. After the electroless Ni-plating, the diffuse emission peak of the original amorphous alloy is almost invisible, replaced by three diffraction peaks corresponding to crystalline Ni. It is suggested that the test surface mainly is composed of crystalline Ni and the BMG substrates cannot be detected, implying that the BMG sample has been well-covered by the Ni coating. It is worth noting that the diffraction peaks of crystalline Ni coating have a large value of width. According to Scherrer equation:

$$D = \frac{0.89\lambda}{\beta \cos \theta} \quad (1)$$

where D is the average size of particles/grains, λ is the wavelength of the used X-ray, β is the full width at half maximum (FWHM) of the peak, and θ is incident angle of the X-ray. By substituting the relevant data measured from the XRD spectrum into Equation (1), the size of the Ni-P particle is calculated to be ~ 122 nm, which is smaller than the results, as observed in Figure 2. When considering that the calculation using Scherrer equation usually shows a large error, the present result is reasonable and consistent with the experimental observation.

It is interesting that the Ni-P coating is a crystalline coating, while not an amorphous one. It can be attributed to the addition of MoO_4^{2-} in the bath, which makes the reaction turn complicated. The introduction of Mo also changes the chemical composition of the deposited coating, as shown in Figure 3c, reducing the GFA of the alloy and resulting in the formation of crystalline phase instead of

amorphous phase. In addition, the addition of MoO_4^{2-} is also responsible for the grain refinement of the coating. The mixing of MoO_4^{2-} in the bath decreases the growth rate of the Ni-P particles, leading to a fine grain structure [36].

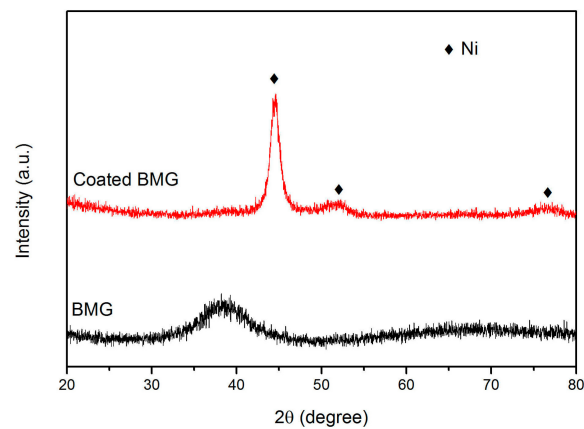


Figure 4. The X-ray diffractometer (XRD) spectra of the Ti-based BMG rod before and after electroless Ni plating.

3.2. Effect of Ni-Coating on the Mechanical Behavior of Ti-Based BMG

Figure 5 displays the compression stress-strain curves of the as-cast and coated BMG samples, respectively. Mechanical properties, including the yield strength $\sigma_{0.2}$, fracture strength σ_y , plastic strain ϵ_p , and elastic modulus E are measured from the stress-strain curves and listed in Table 1.

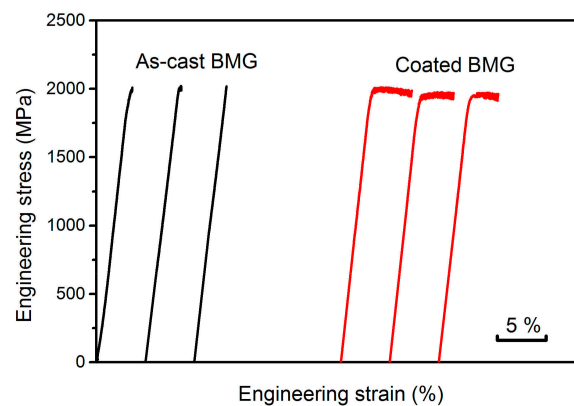


Figure 5. The compression engineering stress-strain curves of the Ni-coated BMG samples together with the as-cast Ti-based bulk metallic glasses (BMG) samples.

Table 1. The mechanical properties of the as-cast bulk metallic glasses (BMG) samples and the coated BMG samples measured from the stress-strain curves.

Status	Number	$\sigma_{0.2}$ (MPa)	σ_y (MPa)	ϵ_p (%)	E (GPa)
As-cast	1	2014	2014	0.46	68
	2	2028	2030	0.52	60
	3	2023	2023	0	62
	average	2021 ± 7	2022 ± 8	0.33 ± 0.28	63.3 ± 4.2
Coated	4	1995	1995	4.31	66
	5	1959	1981	3.71	63
	6	1953	1978	3.08	62
	average	1969 ± 22	1984 ± 9	3.70 ± 0.62	63.2 ± 2.1

For the as-cast samples, the measured values of $\sigma_{0.2}$, σ_y , ϵ_p and E are in accordance with the earlier work [12]. For the coated samples, the measured value of $\sigma_{0.2}$ and σ_y , are decreased about 50 MPa, nearly 2.5% of the total strength. It can be attributed to the enlarged diameters caused by the presence of the Ni-coating with a thickness of about 10 μm , resulting in the measured diameter values for calculation of the engineering stresses to be increased by about 1%. For the E values that are obtained from the curves, there is no obvious change before and after the electroless plating. Although the E values that are measured from the compression stress-strain curves are not accurate than the directly tested ones by ultrasound method. In consideration of the same test condition used for all samples, the E data shown in Table 1 are valuable for comparing the difference between the coated and un-coated samples. At least, it is suggested that the stiffness of the Ti-based BMGs is not obviously affected (or does not turn worse) by the Ni-coating on the surface. For plastic strain, the measured ϵ_p value of the as-cast sample is about $0.33 \pm 0.28\%$, comparable to that in the earlier work [12]. After electroless plating, the coated sample has an improved ϵ_p of $3.70 \pm 0.62\%$, with an increment of 1100%. Therefore, the effect of electroless Ni coating on the plastic deformation capability is significant.

Figure 6 shows the side-view image of the ruptured Ni-coated BMG sample with a ϵ_p value of 4.3%. In general, Ti-based BMG samples are broken in half after compression. Figure 6a shows the overall image of the bottom part of the ruptured sample, in which the fracture angle is about 45° . On the side of the fracture sample, most of the coating has been peeled off, instead by many shear bands, as shown in Figure 6b. The primary shear bands are distributed along the fracture angle in the 45° directions, while the secondary shear bands display in the other directions. In fact, the shear bands observed in the side as shown in Figure 6 are the shear steps caused by shear banding. The formation of the shear steps performs a large peeling force and makes the coating separate from the sample. However, in local areas of the sample, some residual Ni-coating can be observed as adhering to the BMG sample, as marked by the white arrows in Figure 6c,d. Although the residual coatings have been sheared off and penetrated by the shear steps marked by yellow arrows, they still remain being attached to the substrate, indicating that the coatings are very tightly bonded to the substrate. In addition, it is interesting that there are a number of circular spots on the residual coating, with a diameter of $\sim 5 \mu\text{m}$. The composition of the spotted region is similar with that of BMG rod (examined by EDS, the results are not shown here), demonstrating that the spots actually are the parts of the BMG substrate, due to the exposure that is caused by the partially peeling off of the Ni-coating. It is worth to note that the size of the spots is nearly three times bigger than the average size of the Ni particles in the outer coating as shown in Figure 2b. If the spots are taken as the marks of the individual Ni particles/grains to be peeled off, it indicates that there must be certain amount of Ni particles with a size of $5 \mu\text{m}$ or more in the as-plated electroless Ni coating.

Figure 7 shows the fracture surface images of typical Ni-coated BMG sample, taking from the upper part of the ruptured sample with $\epsilon_p = 4.3\%$. There is a cast pore on the middle region of the fracture surface. In general, cast pores can affect the plastic deformation behavior of the sample, resulting in the reduced plastic strains [35]. However, the coated BMG sample still has a high plastic strain value of up to 4.3%, which can be related to the presence of the Ni-coating. Figure 7b shows a high magnification image of the rectangular region that is marked by A, as shown in Figure 7a. It can be clearly seen that region A is in the edge of the fracture surface and there is a light gray layer with a thickness of about $1 \mu\text{m}$ on the side of the ruptured sample. Figure 7d shows the EDS spectrum that was performed on the red cross marked by C, as shown in Figure 7b. The Ni and P peak are obviously higher than the others, demonstrating that the light gray layer is rich in Ni and P. Moreover, the quantitative test results for different elements, as shown in the inset of Figure 7d are similar with that of as-plating coating as shown in the inset of Figure 3c. Therefore, it is suggested that the light gray layer is the residual Ni coating, remaining on the surface after the peeling off of the main Ni-coating from the BMG rod during the compression deformation.

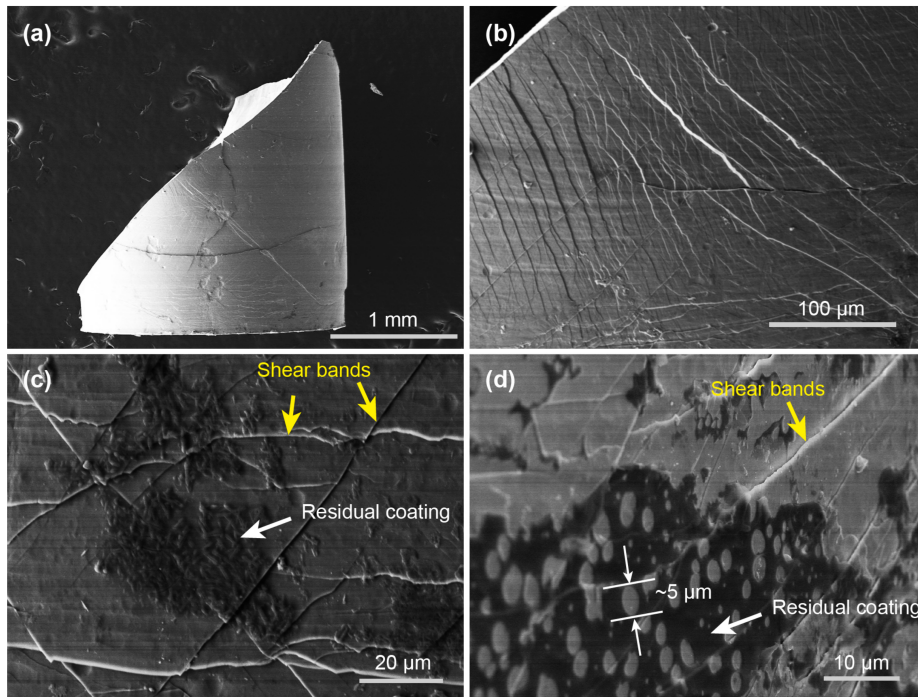


Figure 6. The SEM images showing the side of typical Ni-coated BMG sample after fracture. (a) The overall image of the bottom part of the ruptured sample after compression; (b) Higher magnification image showing multiple shear bands; (c) Residual coating on the surface; and, (d) Peeling trace of the coating in the residual coating.

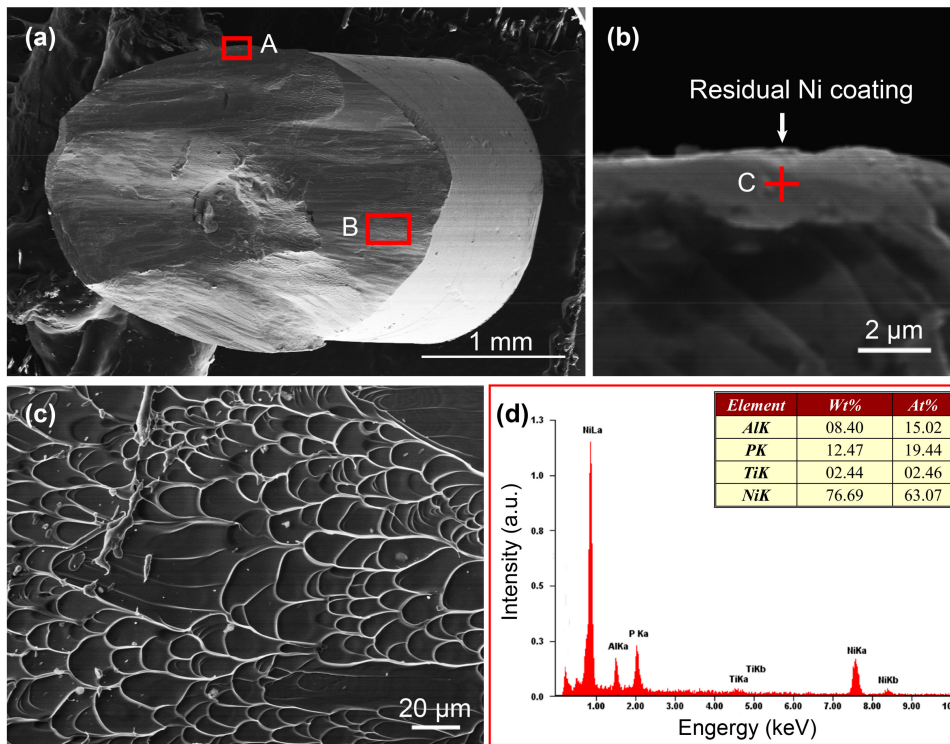


Figure 7. (a) The overall SEM images of the fracture surface of typical Ni-coated BMG sample after fracture; (b) High magnification image of the red square marked by A in (a); (c) Vein like pattern in region B of (a); and, (d) EDS spectrum of cross C in (b).

In addition, typical vein-like pattern can be observed on the smooth fracture surface, as shown in Figure 7c, which is the high-magnification image taking on the region B as marked in Figure 7a. The width and length of the vein unit are well consistent with that of the non-coated BMG sample has been shown in the earlier work elsewhere [12]. It is suggested that the shear banding and fracture behavior of the Ni-coated BMG sample is similar with the as-cast BMG sample, showing typical features of sticky-slip movement [37,38].

4. Discussion

4.1. Role of Thin Ni-Coating on the Shear Banding and Fracture Behavior of Ti-Based BMG

The plastic deformation of BMGs depends on the shear band nucleation and the shear band propagation, and a great amount of shear bands can induce homogeneously plastic deformation [25,39]. Normally, the primary shear band nucleates starting at the surface of BMG samples and rapidly propagates to the inside [40], resulting in no further shear banding elsewhere inside the BMG sample. Since surface defects often induce great stress concentrations, the shear band nucleation tends to occur at a nominal stress much lower than the yield strength of the BMG. In addition, if the propagation of the premature shear bands cannot be suppressed in time, the shear banding will rapidly penetrate the entire sample, achieving highly localized plastic deformation [41].

The role of electroless thin Ni-coating on the deformation behavior of coated BMG lies in two aspects. On the one hand, the presence of the thin Ni-coating reduces the degree of stress concentrations that are caused by bigger surface defects, according to the finite element simulation analysis results, as shown elsewhere in [24]. It is known that the growth of electroless plating coating is generally preferred to the local surface with high surface energy, i.e., on the surface defects. Therefore, the growth of the electroless plating coating itself actually is a selective modification on the surface defects. It is beneficial to limit the localized shear band nucleation upon the bigger defect in the initial stage of the deformation. Furthermore, as the applied load is increased, the surface stresses in different region of the coated BMG sample can simultaneously increase to the critical value to stimulate the uniform nucleation of shear bands. As a result, the multiple shear bands are formed on the surface of the coated BMG sample as shown in Figure 6. On the other hand, the presence of Ni coating can suppress the fast propagation of shear bands. In compression deformation, the surface of the sample usually has a lateral expansion, and the tensile expansion stress on the surface can be released by the formation of shear steps. The Ni coating can limit the lateral expansion deformation, delaying the formation of shear steps and making the primary shear surface be curved. From the overall image Figure 7a, it can be clearly observed that the fracture surface is not a single plane, but a curved surface that is composed by several smaller planes. It indicates that there are multiple shear planes inside the sample as it fractures. Or the primary shear surface is curved before the catastrophic failure, due to the geometric constrain applied by the Ni coating. Then, the local plastic deformation is transformed into the whole plastic deformation, under the combined action of the excitation of multiple shear band nucleation and the deflection shear propagation behavior by geometrical restriction.

4.2. Peeling Mechanism of the Ni-Coating

For electroless plating, the roughening pretreatment is an important process to control the microstructure and properties of the coating. The roughening treatment usually is a corrosion process of the surface to be plated. Since Ti-based BMGs are corrosion-resistant metal materials [6,7], it is relatively hard to uniformly etch the surface of Ti-based BMGs. If the roughening process itself is not uniform, later, the growth of the coating also is inhomogeneous, which might cause the formation of some large Ni particles. In our opinion, the large Ni particles tend to form tensile stress at the interface between the Ni coating and the BMG substrate, as shown in Figure 8.

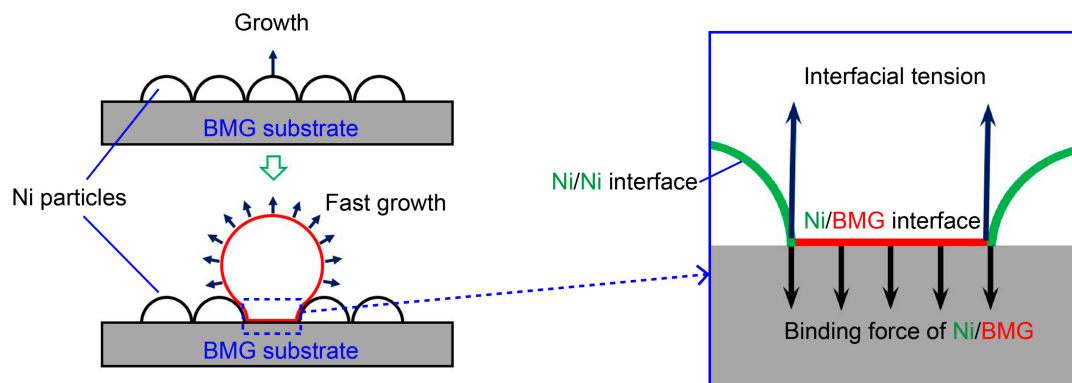


Figure 8. Schematic diagram showing the formation of tensile stress on the interface between the coating and the BMG substrate caused by the abnormal growth of nickel particles during electroless nickel plating.

In the early stage of the electroless plating, the Ni particles mainly grow up depending on the Pd atoms that are attached on the BMG surface during the activation treatment. Since the earlier roughening is inhomogeneous, the sensitization-activation is also inhomogeneous and the Pd atoms are unevenly distributed on the BMG substrate. The region without Pd atoms will be covered by the lateral growth of the neighbor Ni nuclei, and will therefore cause abnormal growth of localized Ni particles. In addition, the growth of Ni particles along the direction perpendicular to the substrate is also not uniform. Some of the Ni particles grow faster than the others, leading to the formation of abnormally grown Ni particles (as shown in Figure 2b, several Ni particles have grown to $\sim 2 \mu\text{m}$). Moreover, as the abnormal Ni particle continues to grow up, the interface between the fast growing Ni particle and the surrounding particles (Ni/Ni interface) will generate an increasingly tensile stress, reversed to the bonding force between the Ni particle and the BMG substrate (Ni/BMG interface). If the tensile stress is beyond the Ni/BMG bonding force, it will stimulate the formation of cracks at the Ni/BMG interface, resulting in the peeling off of the Ni coating. Therefore, avoiding the formation of abnormal grown Ni particles is beneficial for improving the Ni/BMG bonding force. Furthermore, ultrafine coating has good toughness and is helpful to improve the geometric constraint effect of the coating. When compared with the coarser coating, finer coating has a higher amount of grains being oriented in such a manner that sliding systems can be activated, thus improving the ductility and the geometric constrain ability of the coating.

It is suggested that, for electroless nickel plating, improving the binding force between the coating and the substrate has a better geometric restriction effect than such strategy that simply increase the thickness of the coating. In future work, the studies on improving the bonding force between the Ni coating and the Ti-based BMG should be carried out. It is an important research direction to prepare a transition layer that has a stronger binding force with Ti-based BMG matrix. In addition, common methods for grain refinement and composition adjustment still require further study to find the best processing parameters based on Ti-based BMGs.

5. Conclusions

In the present work, the traditional electroless Ni plating is introduced to the study on plasticity improvement of Ti-based BMGs at room temperature. It is found that a two-layered thin crystalline Ni coating can be prepared on the surface of mechanically ground $\text{Ti}_{37.31}\text{Zr}_{22.75}\text{Be}_{25.48}\text{Fe}_{5.46}\text{Cu}_9$ BMG, following the process route proposed in the experiment. The thickness of the outer layer of the Ni coating is about $10 \mu\text{m}$ and the grain size is between $\sim 500 \text{ nm}$ to $\sim 5 \mu\text{m}$; the thickness of the inner layer is only about $1 \mu\text{m}$ with a grain size of about 100 nm . The coating causes the formation of a number of shear bands on the surface of the deformed sample, indicating that the coating can availably limits the shear band propagation and effectively stimulates the shear band nucleation. As a result,

the plastic strain of the Ti-based BMG is significantly improved from 0.3% to 3.7%, with an increase of over 1100%. Most of the coating is peeled off from the substrate after the rupture, which can be attributed to the structural inhomogeneity of the Ni coating. Abnormally coarse Ni particles induce an increasing tensile stress between the Ni coating and the BMG substrate, resulting in the peeling off of the coating. It is suggested that, for electroless nickel plating, improving the adhesive bonding strength between the coating and the substrate has a better geometric restriction effect than by simply increasing the thickness. In the future work, further studies on grain refinement and transition layer are needed to improve the bonding strength of electroless Ni coatings and Ti-based BMGs.

Acknowledgments: This work was financially supported by Science and Technology Research Projects for Colleges and Universities presented by Hebei Education Department of China (Grant No. QN2014032), Hebei Province High-level Talent Founding Projects presented by Hebei Provincial Department of Human Resources and Social Security of China (Grant No. B2015003012) and Natural Science Foundation of Hebei Province in China (Grant Nos. E2016202332 and E2016202406).

Author Contributions: Xin Wang and Chunxiang Cui conceived and designed the experiments; Xin Wang, Ximei Hu, Dongxu Jiang, Peng Chen, Pengdong Wang and Zhipeng Zhang performed the experiments; Xin Wang, Lichen Zhao, and Chunxiang Cui analyzed the data; Shuiqing Liu contributed materials tools; Xin Wang and Chunxiang Cui wrote the paper.

Conflicts of Interest: The authors declare no conflict of interest.

References

1. Kim, Y.C.; Kim, W.T.; Kim, D.H. A development of Ti-based bulk metallic glass. *Mater. Sci. Eng. A* **2004**, *375–377*, 127–135. [[CrossRef](#)]
2. Duan, G.; Wiest, A.; Lind, M.L.; Kahl, A.; Johnson, W.L. Lightweight Ti-based bulk metallic glasses excluding late transition metals. *Scr. Mater.* **2008**, *58*, 465–468. [[CrossRef](#)]
3. Park, J.M.; Wang, G.; Pauly, S.; Mattern, N.; Kim, D.H.; Eckert, J. Ductile Ti-Based Bulk Metallic Glasses with High Specific Strength. *Metall. Mater. Trans. A* **2011**, *42*, 1456–1462. [[CrossRef](#)]
4. Gong, P.; Yao, K.F.; Wang, X.; Shao, Y. Centimeter-sized Ti-based bulk metallic glass with high specific strength. *Prog. Nat. Sci. Mater.* **2012**, *22*, 401–406. [[CrossRef](#)]
5. Gong, P.; Yao, K.; Wang, X.; Shao, Y. A New Centimeter-Sized Ti-Based Quaternary Bulk Metallic Glass with Good Mechanical Properties. *Adv. Eng. Mater.* **2013**, *15*, 691–696. [[CrossRef](#)]
6. Morrison, M.L.; Buchanan, R.A.; Peker, A.; Liaw, P.K.; Horton, J.A. Electrochemical behavior of a Ti-based bulk metallic glass. *J. Non-Cryst. Solids* **2007**, *353*, 2115–2124. [[CrossRef](#)]
7. Gu, J.-L.; Shao, Y.; Zhao, S.-F.; Lu, S.-Y.; Yang, G.-N.; Chen, S.-Q.; Yao, K.-F. Effects of Cu addition on the glass forming ability and corrosion resistance of Ti-Zr-Be-Ni alloys. *J. Alloys Compd.* **2017**, *725*, 573–579. [[CrossRef](#)]
8. Zhu, S.L.; Wang, X.M.; Qin, F.X.; Yoshimura, M.; Inoue, A. New TiZrCuPd Quaternary Bulk Glassy Alloys with Potential of Biomedical Applications. *Mater. Trans.* **2007**, *48*, 2445–2448. [[CrossRef](#)]
9. Wang, G.; Fan, H.B.; Huang, Y.J.; Shen, J.; Chen, Z.H. A new TiCuHfSi bulk metallic glass with potential for biomedical applications. *Mater. Des.* **2014**, *54*, 251–255. [[CrossRef](#)]
10. Pang, S.; Liu, Y.; Li, H.; Sun, L.; Li, Y.; Zhang, T. New Ti-based Ti-Cu-Zr-Fe-Sn-Si-Ag bulk metallic glass for biomedical applications. *J. Alloys Compd.* **2015**, *625*, 323–327. [[CrossRef](#)]
11. Tang, M.Q.; Zhang, H.F.; Zhu, Z.W.; Fu, H.M.; Wang, A.M.; Li, H.; Hu, Z.Q. TiZr-base Bulk Metallic Glass with over 50 mm in Diameter. *J. Mater. Sci. Technol.* **2010**, *26*, 481–486. [[CrossRef](#)]
12. Gong, P.; Wang, X.; Shao, Y.; Chen, N.; Liu, X.; Yao, K. A Ti-Zr-Be-Fe-Cu bulk metallic glass with superior glass-forming ability and high specific strength. *Intermetallics* **2013**, *43*, 177–181. [[CrossRef](#)]
13. Telford, M. The case for bulk metallic glasses. *Mater. Today* **2004**, *7*, 36–43. [[CrossRef](#)]
14. Nishiyama, N.; Amiya, K.; Inoue, A. Novel applications of bulk metallic glass for industrial products. *J. Non-Cryst. Solids* **2007**, *353*, 3615–3621. [[CrossRef](#)]
15. Gong, P.; Wang, X.; Shao, Y.; Chen, N.; Yao, K.F. Ti-Zr-Be-Fe quaternary bulk metallic glasses designed by Fe alloying. *Sci. China Phys. Mech.* **2013**, *56*, 2090–2097. [[CrossRef](#)]
16. Gong, P.; Wang, X.; Yao, K.F. Effects of alloying elements on crystallization kinetics of Ti-Zr-Be bulk metallic glass. *J. Mater. Sci.* **2016**, *51*, 5321–5329. [[CrossRef](#)]

17. Wang, X.; Shao, Y.; Gong, P.; Yao, K.F. The effect of simulated thermal cycling on thermal and mechanical stability of a Ti-based bulk metallic glass. *J. Alloys Compd.* **2013**, *575*, 449–454. [[CrossRef](#)]
18. Nieh, T.; Yang, Y.; Lu, J.; Liu, C. Effect of surface modifications on shear banding and plasticity in metallic glasses: An overview. *Prog. Nat. Sci. Mater.* **2012**, *22*, 355–363. [[CrossRef](#)]
19. Zhang, Y.; Wang, W.H.; Greer, A.L. Making metallic glasses plastic by control of residual stress. *Nat. Mater.* **2006**, *5*, 857–860. [[CrossRef](#)] [[PubMed](#)]
20. Wang, Q.; Yang, Y.; Jiang, H.; Liu, C.; Ruan, H.; Lu, J. Superior Tensile Ductility in Bulk Metallic Glass with Gradient Amorphous Structure. *Sci. Rep.* **2014**, *4*, 4757. [[CrossRef](#)] [[PubMed](#)]
21. Chu, J.P.; Greene, J.E.; Jang, J.S.C.; Huang, J.C.; Shen, Y.-L.; Liaw, P.K.; Yokoyama, Y.; Inoue, A.; Nieh, T.G. Bendable bulk metallic glass: Effects of a thin, adhesive, strong, and ductile coating. *Acta Mater.* **2012**, *60*, 3226–3238. [[CrossRef](#)]
22. Chen, B.; Li, Y.; Yi, M.; Li, R.; Pang, S.; Wang, H.; Zhang, T. Optimization of mechanical properties of bulk metallic glasses by residual stress adjustment using laser surface melting. *Scr. Mater.* **2012**, *66*, 1057–1060. [[CrossRef](#)]
23. Li, H.; Li, L.; Fan, C.; Choo, H.; Liaw, P.K. Nanocrystalline coating enhanced ductility in a Zr-based bulk metallic glass. *J. Mater. Res.* **2007**, *22*, 508–513. [[CrossRef](#)]
24. Li, J.-F.; Wang, X.; Yang, G.-N.; Chen, N.; Liu, X.; Yao, K.-F. Enhanced plasticity of a Fe-based bulk amorphous alloy by thin Ni coating. *Mater. Sci. Eng. A* **2015**, *645*, 318–322. [[CrossRef](#)]
25. Greer, A.L.; Cheng, Y.Q.; Ma, E. Shear bands in metallic glasses. *Mater. Sci. Eng. R* **2013**, *74*, 71–132. [[CrossRef](#)]
26. Steif, P.S.; Spaepen, F.; Hutchinson, J.W. Strain localization in amorphous metals. *Acta. Metall.* **1982**, *30*, 447–455. [[CrossRef](#)]
27. Yu, P.; Liu, Y.H.; Wang, G.; Bai, H.Y.; Wang, W.H. Enhance plasticity of bulk metallic glasses by geometric confinement. *J. Mater. Res.* **2007**, *22*, 2384–2388. [[CrossRef](#)]
28. Qiu, S.B.; Yao, K.F. Novel application of the electrodeposition on bulk metallic glasses. *Appl. Surf. Sci.* **2008**, *255*, 3454–3458. [[CrossRef](#)]
29. Chen, W.; Chan, K.C.; Chen, S.H.; Guo, S.F.; Li, W.H.; Wang, G. Plasticity enhancement of a Zr-based bulk metallic glass by an electroplated Cu/Ni bilayered coating. *Mater. Sci. Eng. A* **2012**, *552*, 199–203. [[CrossRef](#)]
30. Ren, L.W.; Meng, M.M.; Wang, Z.; Yang, F.Q.; Yang, H.J.; Zhang, T.; Qiao, J.W. Enhancement of plasticity in Zr-based bulk metallic glasses electroplated with copper coatings. *Intermetallics* **2015**, *57*, 121–126. [[CrossRef](#)]
31. Balaraju, J.N.; Kalavati; Rajam, K.S. Influence of particle size on the microstructure, hardness and corrosion resistance of electroless Ni-P-Al₂O₃ composite coatings. *Surf. Coat. Technol.* **2006**, *200*, 3933–3941. [[CrossRef](#)]
32. Krishnan, K.H.; John, S.; Srinivasan, K.N.; Praveen, J.; Ganesan, M.; Kavimani, P.M. An overall aspect of electroless Ni-P depositions—A review article. *Metall. Mater. Trans. A* **2006**, *37*, 1917–1926. [[CrossRef](#)]
33. Ren, L.W.; Wang, Z.; Meng, M.M.; Tian, H.; Yang, H.J.; Qiao, J.W. Plasticity enhancement in bulk metallic glasses by electroless plating with Ni-P amorphous films. *J. Non-Cryst. Solids* **2015**, *430*, 115–119. [[CrossRef](#)]
34. Cao, J.W.; Han, J.G.; Guo, Z.H.; Zhao, W.B.; Guo, Y.Q.; Xia, Z.H.; Qiao, J.W. Plasticity enhancement of high-entropy bulk metallic glasses by electroless plating with Ni-P amorphous films. *Mater. Sci. Eng. A* **2016**, *673*, 141–147. [[CrossRef](#)]
35. Wang, X.; Gong, P.; Yao, K.F. Mechanical behavior of bulk metallic glass prepared by copper mold casting with reversed pressure. *J. Mater. Proc. Technol.* **2016**, *237*, 270–276. [[CrossRef](#)]
36. Lu, G.J.; Zangari, G. Study of the electroless deposition process of Ni-P-based ternary alloys. *J. Electrochem. Soc.* **2003**, *150*, 777–786. [[CrossRef](#)]
37. Torre, F.H.D.; Klaumünzer, D.; Maaß, R.; Löffler, J.F. Stick-slip behavior of serrated flow during inhomogeneous deformation of bulk metallic glasses. *Acta Mater.* **2010**, *58*, 3742–3750. [[CrossRef](#)]
38. Sun, B.A.; Pauly, S.; Tan, J.; Stoica, M.; Wang, W.H.; Kühn, U.; Eckert, J. Serrated flow and stick-slip deformation dynamics in the presence of shear band interaction in a Zr-based bulk metallic glass. *Acta Mater.* **2013**, *60*, 4160–4171, Corrigendum in **2013**, *61*, 2281. [[CrossRef](#)]
39. Yao, K.F.; Ruan, F.; Yang, Y.Q.; Chen, N. Superductile bulk metallic glass. *Appl. Phys. Lett.* **2006**, *88*, 122106. [[CrossRef](#)]

40. Wang, G.; Feng, Q.; Yang, B.; Jiang, W.; Liaw, P.K.; Liu, C.T. Thermographic studies of temperature evolutions in bulk metallic glasses: An overview. *Intermetallics* **2012**, *30*, 1–11. [[CrossRef](#)]
41. Lewandowski, J.J.; Greer, A.L. Temperature rise at shear bands in metallic glasses. *Nat. Mater.* **2006**, *5*, 15–18. [[CrossRef](#)]



© 2017 by the authors. Licensee MDPI, Basel, Switzerland. This article is an open access article distributed under the terms and conditions of the Creative Commons Attribution (CC BY) license (<http://creativecommons.org/licenses/by/4.0/>).